AE4304P: Stochastic Aerospace Systems Practical

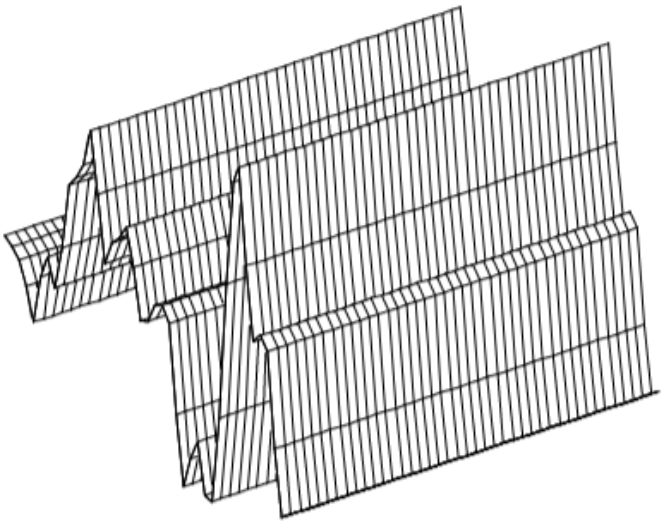

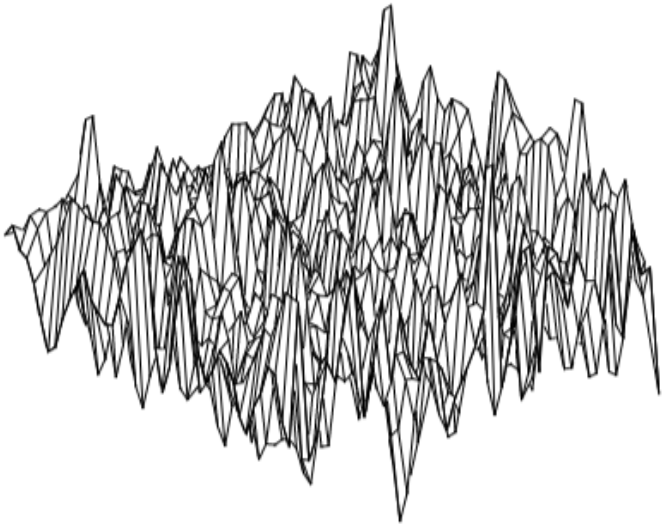

TU Delft

AE4304P: Stochastic Aerospace Systems Practical

by

Student Name	Student Number
Justas Andriuskevicius	5062632

Contents

1
Introduction

In the field of aerospace engineering, understanding aircraft responses to atmospheric turbulence is of paramount importance for ensuring safety and optimising flight performance. The objective of this report is to present a detailed investigation of aircraft responses to symmetrical vertical and longitudinal atmospheric turbulence using time and frequency domain analysis techniques, with a focus on their practical application, advantages, disadvantages, and limitations. Calculations performed for both the complete set of equations of motion and the equations of motion for the short-period assumption. The report is divided into four parts: stability analysis, time-domain analysis, spectral analysis, and estimation of variances.

Several assumptions are taken into account when modelling turbulence [1]:

- Gaussian distribution assumption: Atmospheric turbulence is often assumed to be a random process with a Gaussian distribution, which simplifies the analysis. This assumption is considered valid in many practical situations.
- Stationary process: Atmospheric turbulence is assumed to be a stationary process because aircraft typically fly at speeds much higher than turbulence velocities, which allows them to traverse large patches of turbulence in a short time without encountering significant changes in turbulence velocities. This leads to the simplification of the correlation and spectral density matrices, known as Taylor's hypothesis.
- Homogeneity along the flight path: Turbulence is considered to be homogeneous along the flight path, especially at high altitudes where large patches of turbulence can be found. This approximation is reasonable for aircraft in nearly horizontal flight, which further simplifies the covariance and spectral density matrices. This assumption also implies that the turbulence is ergodic, allowing time averages to replace ensemble averages in practical applications.
- Isotropic process: Atmospheric turbulence is assumed to be isotropic, particularly at high altitudes, meaning that all statistical properties are independent of the orientation of the axes. This assumption simplifies the analysis of turbulence and is supported by evidence from high-altitude measurements.

The conditions provided for the turbulence is as follows:

$$L_g = 150m, \sigma_{u_g} = 2m/s, \sigma_{w_g} = 2m/s \tag{1.1}$$

Through the completion of this assignment, the aim to not only deepen the understanding of aircraft dynamics in turbulent conditions but also to highlight the versatility of the time and frequency domain analysis techniques in examining various stochastic processes.

2

Stability Analysis

In this chapter, stability analysis is explored for two aircraft models: the full set of equations of motion and the equations of motion based on the short-period assumption. The aircraft's response to the combined simulation of vertical and longitudinal turbulence is assessed using the previously mentioned conditions (Equation 1.1). The state space mode is referred to as:

$$\begin{aligned} \dot{x} &= Ax + B \\ y &= Cx + Du \end{aligned} \tag{2.1}$$

The full state space is given in Equation 2.2 where A and B matrices can be seen [1], while C matrix is 7x7 identity matrix and D matrix is 7x3 null matrix.

$$\begin{bmatrix} \dot{\hat{u}} \\ \dot{\alpha} \\ \dot{\theta} \\ \frac{\dot{q}\bar{c}}{V} \\ \dot{\hat{u}}_g \\ \dot{\alpha} \\ \dot{\alpha}_g^* \end{bmatrix} = \begin{bmatrix} x_u & x_\alpha & x_\theta & 0 & x_{u_g} & x_{\alpha_g} & 0 \\ z_u & z_\alpha & z_\theta & z_q & z_{u_g} - z_{\dot{u}_g}\frac{V}{L_g}\frac{\bar{c}}{V} & z_{\alpha_g} & z_{\dot{\alpha}_g}\frac{\bar{c}}{V} \\ 0 & 0 & 0 & \frac{V}{\bar{c}} & 0 & 0 & 0 \\ m_u & m_\alpha & m_\theta & m_q & m_{u_g} - m_{\dot{u}_g}\frac{V}{L_g}\frac{\bar{c}}{V} & m_{\alpha_g} & m_{\dot{\alpha}_g}\frac{\bar{c}}{V} \\ 0 & 0 & 0 & 0 & -\frac{V}{L_g} & 0 & 0 \\ 0 & 0 & 0 & 0 & 0 & 0 & 1 \\ 0 & 0 & 0 & 0 & 0 & -\frac{V^2}{{L_g}^2} & -2\frac{V}{L_g} \end{bmatrix} \begin{bmatrix} \hat{u} \\ \alpha \\ \theta \\ \frac{q\bar{c}}{V} \\ \hat{u}_g \\ \alpha_g \\ \alpha_g^* \end{bmatrix} + \\ + \begin{bmatrix} x_{\delta_e} & 0 & 0 \\ z_{\delta_e} & z_{\dot{u}_g}\frac{\bar{c}}{V}\sigma_{\hat{u}_g}\sqrt{\frac{2V}{L_g}} & z_{\dot{\alpha}_g}\frac{\bar{c}}{V}\sigma_{\alpha_g}\sqrt{\frac{3V}{L_g}} \\ 0 & 0 & 0 \\ m_{\delta_e} & m_{\dot{u}_g}\frac{\bar{c}}{V}\sigma_{\hat{u}_g}\sqrt{\frac{2V}{L_g}} & m_{\dot{\alpha}_g}\frac{\bar{c}}{V}\sigma_{\alpha_g}\sqrt{\frac{3V}{L_g}} \\ 0 & \sigma_{\hat{u}_g}\sqrt{\frac{2V}{L_g}} & 0 \\ 0 & 0 & \sigma_{\alpha_g}\sqrt{\frac{3V}{L_g}} \\ 0 & 0 & (1-2\sqrt{3})\sigma_{\alpha_g}\sqrt{\left(\frac{V}{L_g}\right)^3} \end{bmatrix} \begin{bmatrix} \delta_e \\ w_1 \\ w_3 \end{bmatrix} \tag{2.2}$$

The short-period motion involves rapid changes in pitch rate (q) and angle of attack (α), but little change in pitch angle (θ) and forward velocity (u) [2]. The assumption is based on the fact that the short period oscillations are faster than the phugoid motion, which involves significant changes in pitch angle and forward velocity. As a result, the short period motion mainly focuses on the aircraft's pitch rate and angle of attack dynamics. This assumption leads to removing first and third row and column from A and C matrix as well as first and third row from B and D matrix. The reduced A and B matrices are

shown in Equation 2.3, while reduced C matrix is now 5x5 identity matrix and D is 5x3 null matrix. The reduced matrices will be referred with the letter 'r' at the end: Ar, Br, Cr, Dr.

$$\begin{bmatrix} \dot{\alpha} \\ \frac{\dot{q}\bar{c}}{V} \\ \dot{\hat{u}}_g \\ \dot{\alpha} \\ \dot{\alpha}_g^* \end{bmatrix} = \begin{bmatrix} z_\alpha & z_q & z_{u_g} - z_{\dot{u}_g}\frac{V}{L_g}\frac{\bar{c}}{V} & z_{\alpha_g} & z_{\dot{\alpha}_g}\frac{\bar{c}}{V} \\ m_\alpha & m_q & m_{u_g} - m_{\dot{u}_g}\frac{V}{L_g}\frac{\bar{c}}{V} & m_{\alpha_g} & m_{\dot{\alpha}_g}\frac{\bar{c}}{V} \\ 0 & 0 & -\frac{V}{L_g} & 0 & 0 \\ 0 & 0 & 0 & 0 & 1 \\ 0 & 0 & 0 & -\frac{V^2}{{L_g}^2} & -2\frac{V}{L_g} \end{bmatrix} \begin{bmatrix} \alpha \\ \frac{q\bar{c}}{V} \\ \hat{u}_g \\ \alpha_g \\ \alpha_g^* \end{bmatrix} + \\ + \begin{bmatrix} z_{\delta_e} & z_{\dot{u}_g}\frac{\bar{c}}{V}\sigma_{\hat{u}_g}\sqrt{\frac{2V}{L_g}} & z_{\dot{\alpha}_g}\frac{\bar{c}}{V}\sigma_{\alpha_g}\sqrt{\frac{3V}{L_g}} \\ m_{\delta_e} & m_{\dot{u}_g}\frac{\bar{c}}{V}\sigma_{\hat{u}_g}\sqrt{\frac{2V}{L_g}} & m_{\dot{\alpha}_g}\frac{\bar{c}}{V}\sigma_{\alpha_g}\sqrt{\frac{3V}{L_g}} \\ 0 & \sigma_{\hat{u}_g}\sqrt{\frac{2V}{L_g}} & 0 \\ 0 & 0 & \sigma_{\alpha_g}\sqrt{\frac{3V}{L_g}} \\ 0 & 0 & (1-2\sqrt{3})\sigma_{\alpha_g}\sqrt{\left(\frac{V}{L_g}\right)^3} \end{bmatrix} \begin{bmatrix} \delta_e \\ w_1 \\ w_3 \end{bmatrix} \tag{2.3}$$

By plugging in the numbers the results can be seen below:

$$A = \begin{pmatrix} -0.01913644 & 0.01738226 & -0.05166838 & 0.00000000 & -0.01913644 & 0.01738226 & 0.00000000 \\ -0.10269753 & -1.83841249 & 0.00000000 & 91.80017680 & -0.10269753 & -1.83841249 & 0.00861982 \\ 0.00000000 & 0.00000000 & 0.00000000 & 93.76854600 & 0.00000000 & 0.00000000 & 0.00000000 \\ 0.00174656 & -0.14834842 & 0.00000000 & -4.24704335 & 0.00174656 & -0.14834842 & 0.01148964 \\ 0.00000000 & 0.00000000 & 0.00000000 & 0.00000000 & -1.26400000 & 0.00000000 & 0.00000000 \\ 0.00000000 & 0.00000000 & 0.00000000 & 0.00000000 & 0.00000000 & 0.00000000 & 1.00000000 \\ 0.00000000 & 0.00000000 & 0.00000000 & 0.00000000 & 0.00000000 & -1.59769600 & -2.52800000 \end{pmatrix} \tag{2.4}$$

$$B = \begin{pmatrix} 0.00000000 & 0.00000000 & 0.00000000 \\ -0.18377785 & 0.00000000 & 0.00017706 \\ 0.00000000 & 0.00000000 & 0.00000000 \\ -0.48166429 & 0.00000000 & 0.00023601 \\ 0.00000000 & 0.01677182 & 0.00000000 \\ 0.00000000 & 0.00000000 & 0.02054120 \\ 0.00000000 & 0.00000000 & -0.03693779 \end{pmatrix} \tag{2.5}$$

$$A_r = \begin{pmatrix} -1.83841249 & 91.80017680 & -0.10269753 & -1.83841249 & 0.00861982 \\ -0.14834842 & -4.24704335 & 0.00174656 & -0.14834842 & 0.01148964 \\ 0.00000000 & 0.00000000 & -1.26400000 & 0.00000000 & 0.00000000 \\ 0.00000000 & 0.00000000 & 0.00000000 & 0.00000000 & 1.00000000 \\ 0.00000000 & 0.00000000 & 0.00000000 & -1.59769600 & -2.52800000 \end{pmatrix} \tag{2.6}$$

$$B_r = \begin{pmatrix} -0.18377785 & 0.00000000 & 0.00017706 \\ -0.48166429 & 0.00000000 & 0.00023601 \\ 0.00000000 & 0.01677182 & 0.00000000 \\ 0.00000000 & 0.00000000 & 0.02054120 \\ 0.00000000 & 0.00000000 & -0.03693779 \end{pmatrix} \tag{2.7}$$

The eigenvalues are analysed to determine the stability of the aircraft. The eigenvalues of the full system are presented in Table 2.1 and depicted in Figure 2.1. As evident from the results, there are no eigenvalues with positive real parts, which indicates that the system is stable. Consequently, there is no need to design an autopilot (pitch-damper) for this particular case. A similar conclusion can be drawn for the reduced system, as shown in Table 2.2 and Figure 2.2.

Table 2.1: Eigenvalues of the full system

Eigenvalues of the full system
-3.043 + 3.488i
-3.043 - 3.488i
-0.009285 + 0.06391i
-0.009285 - 0.06391i
-1.264
-1.264
-1.264

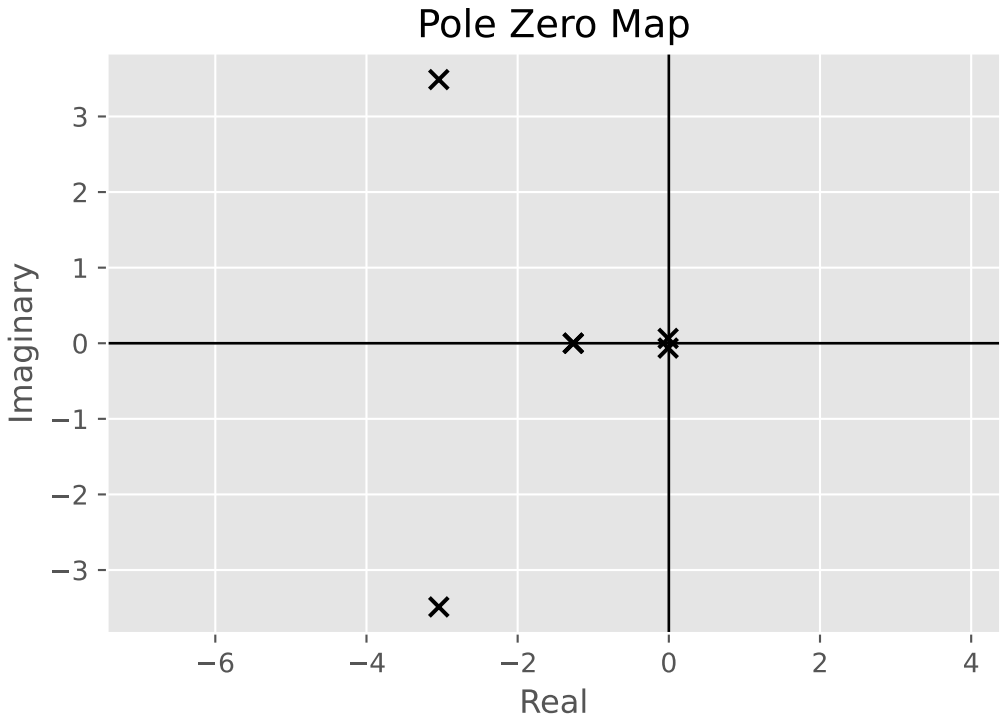

Figure 2.1: Pole-zero plot for the full system

Table 2.2: Eigenvalues of the reduced system

Eigenvalues of the reduced system
-3.043 + 3.488i
-3.043 - 3.488i
-1.264
-1.264
-1.264

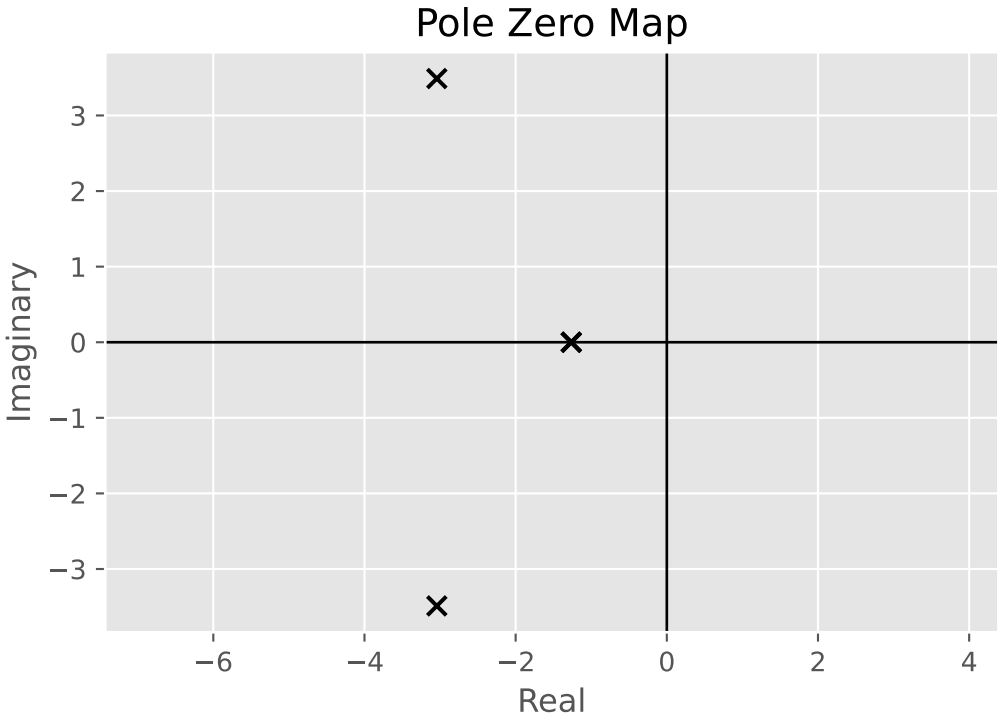

Figure 2.2: Pole-zero plot for the reduced system

3

Time-Domain Analysis

This chapter presents and analyses the time domain simulation results of the aircraft flying through turbulence (combination of vertical and longitudinal turbulence). This includes aircraft states and load factor ($n_z = \frac{a_z}{g}$).

$$a_z = \frac{d^2h}{dt^2} = \frac{d}{dt}Vsin\gamma \approx V\dot{\gamma} = V(\dot{theta} - \dot{\alpha}) = V(\frac{V}{\bar{c}}\frac{q\bar{c}}{V} - \dot{\alpha}) \tag{3.1}$$

The time duration is 60 s and time step is 0.01 s. The elevator input is set to zero. Vertical and longitudinal turbulence input is sampled from a standard normal distribution and divided by the $\sqrt{dt}$ to discretise the process. The output is the simulated with lsim function. Exact same process is done for the reduced system. Below the simulated result can be seen. The load factor (n_z) is has a mean of around 0 and varies from 0.96 to -0.9. The airspeed deviation ($\hat{u}$) varies the least out of all the aircraft states. The angle of attack (α) and pitch angle (θ) varies from around 1.5 to -1 or just below -1 degrees. Finally pitch rate ($q\bar{c}/V$) is around from 0.02 to -0.03 degrees. Similar numbers can be seen for the reduced system as well. Note that radians have been transformed to degrees for the purpose of visualisation.

Figure 3.1: Aircraft load factor Vs. time for full system

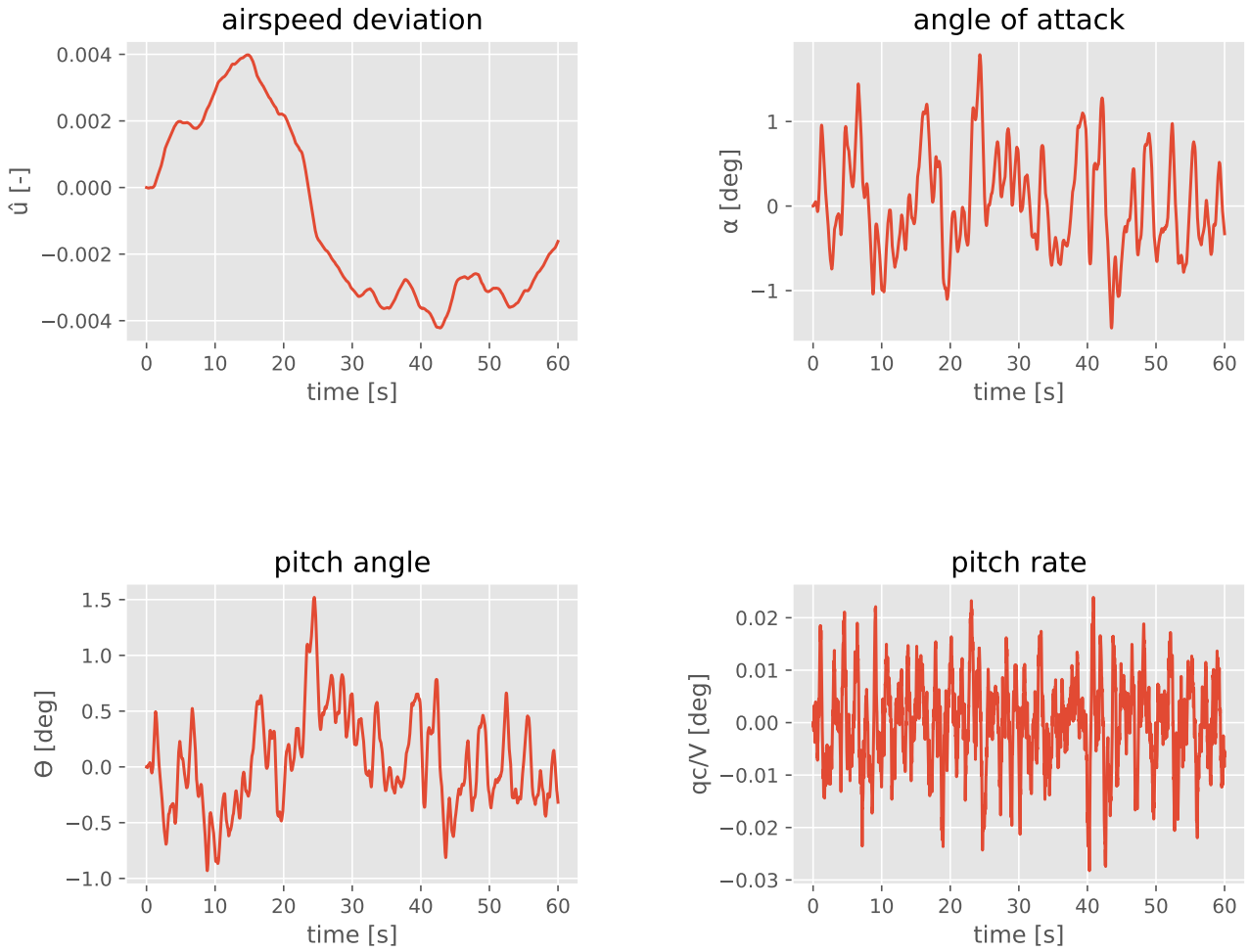

Figure 3.2: Aircraft states Vs. time for full system

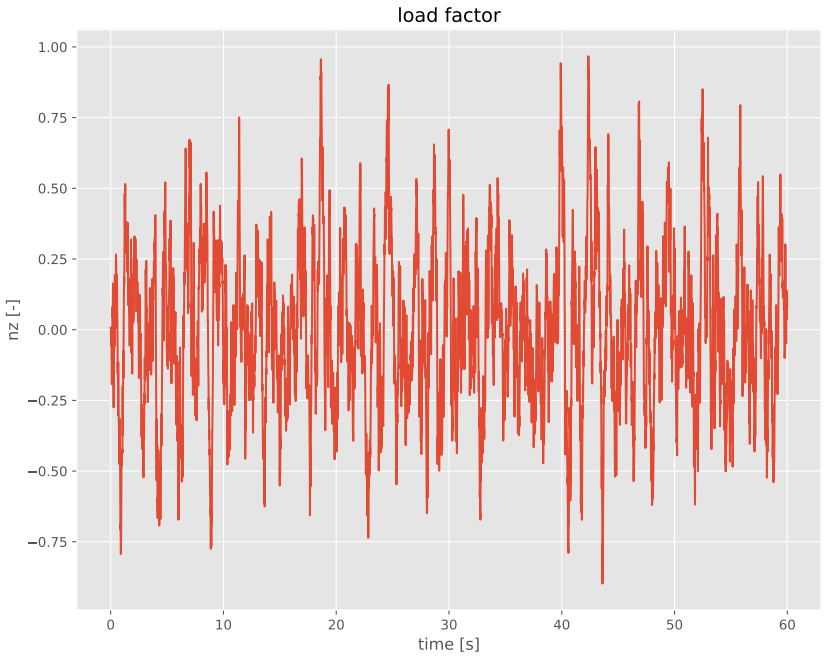

Figure 3.3: Aircraft load factor Vs. time for reduced system

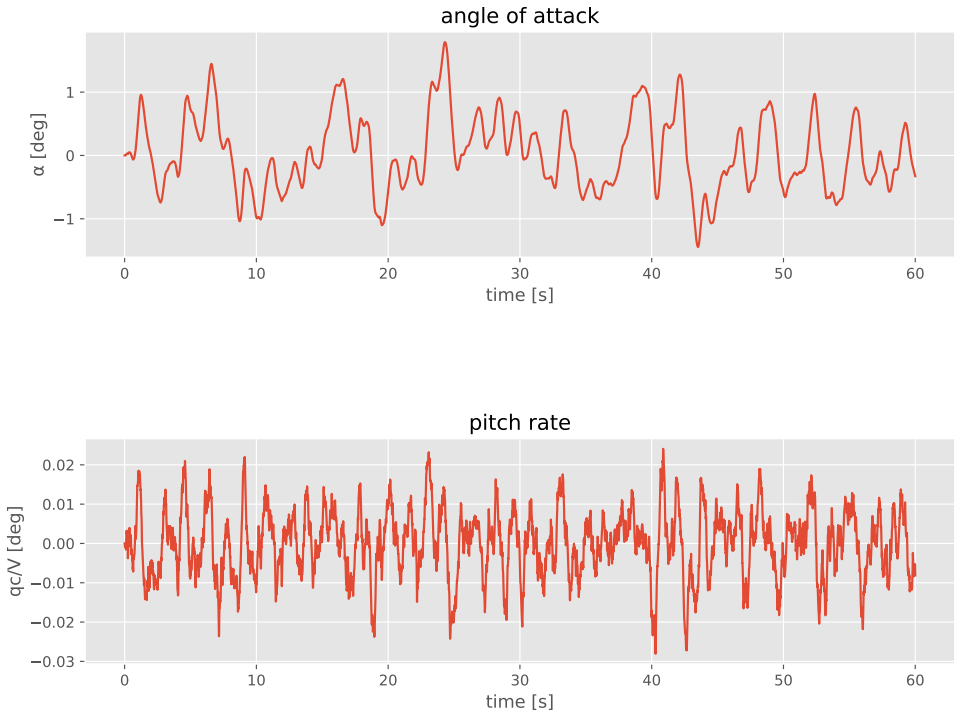

Figure 3.4: Aircraft states Vs. time for reduced system

4

Spectral Analysis

Power spectral density (PSD) quantifies how the power of a signal is distributed over a range of frequencies, providing insights into the dominant frequencies. In this chapter the results of analytical, experimental and smoothed experimental PSDs are presented. The equation for analytical auto-PSD function is shown in Equation 4.1, T is the sampled period and $A(w)$ is the signal magnitude in the frequency domain. $A(w)$ is computed with the bode function. However bode function is currently only implemented for SISO systems (at least in Python). Fortunately, since the two inputs (vertical and longitudinal turbulence) are independent and uncorrelated, means that the two PSDs can be simply added together. Hence for each aircraft state a PSD is generated by using only vertical turbulence, then only longitudinal turbulence and finally summing PSDs together.

$$S_{\bar{x}\bar{x}}(\omega) = \lim_{T\to\infty} \frac{1}{2T}\bar{A}(\omega)\bar{A}(-\omega) = \lim_{T\to\infty} \frac{1}{2T}|\bar{A}(\omega)|^2 \tag{4.1}$$

The experimental PSD is computed by using FFT algorithm (Equation 4.2). To convert from continuous time to discrete time, a scaling factor of $1/dt$ was applied. To reverse this process and convert back to continuous time, the FFT is multiplied by a scaling factor of dt. Finally, the square of the magnitude is divided by the total period to calculate the periodogram (Equation 4.3).

$$\bar{X}[k] = \sum_{n=0}^{N-1} \bar{x}[n]e^{-jk\frac{2\pi}{N}n}, \quad \text{for } k = 0, 1, 2, \dots, N-1 \tag{4.2}$$

$$I_{N\bar{x}\bar{x}}[k] = \frac{1}{N}\bar{X}^*[k]\bar{X}[k] = \frac{1}{N}|\bar{X}[k]|^2 \tag{4.3}$$

Experimental PSD with the smoothing filter is calculated by using Equation 4.4

$$\Phi_{\text{estimate}}\,[k] = 0.25\Phi[k-1] + 0.5\Phi[k] + 0.25\Phi[k+1] \tag{4.4}$$

for only one realisation of the periodogram ($\Phi[k]$ is the periodogram).

The results are presented below, where Figure 4.1 and Figure 4.2 presents PSDs of aircraft states for full system and reduced system respectively. In Figure 4.3 and Figure 4.4 shows PSD of load factor for full and reduced system. Firstly, differences were found between the three calculation methods (Equation 4.1, Equation 4.3 and Equation 4.4) for the PSD.

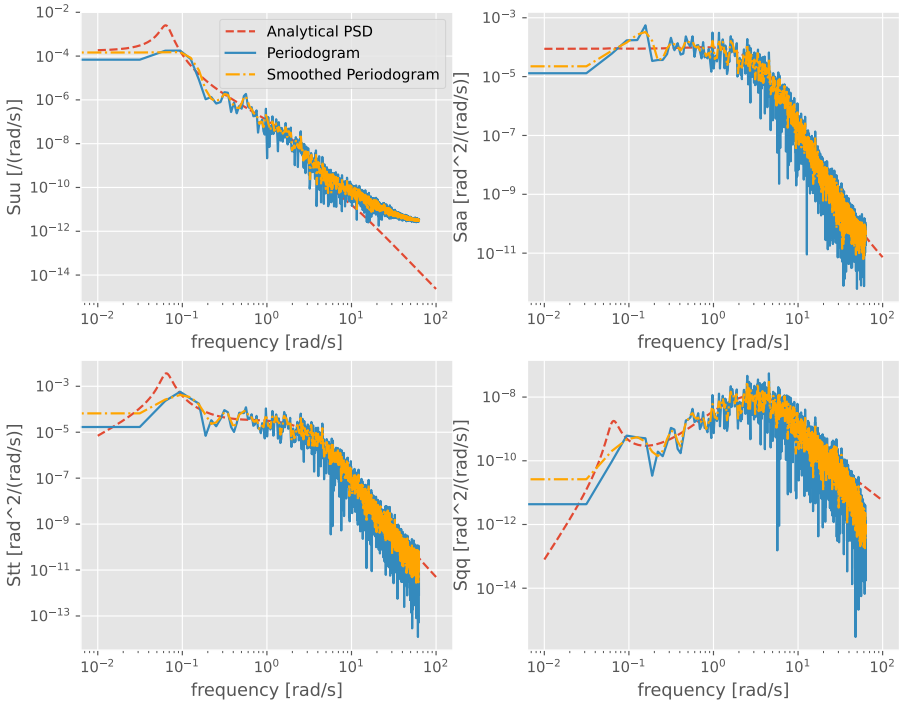

Figure 4.1: PSDs of aircraft states for full system

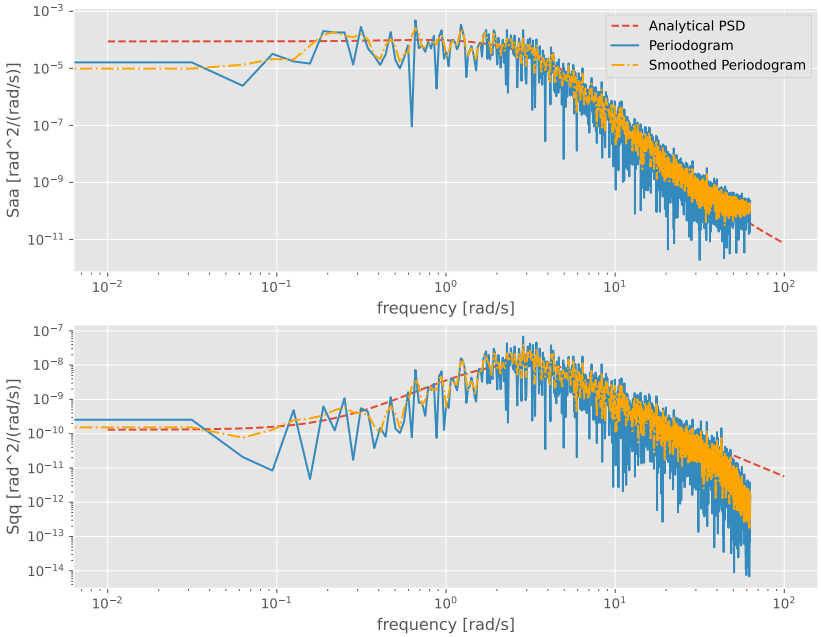

Figure 4.2: PSDs of aircraft states for reduced system

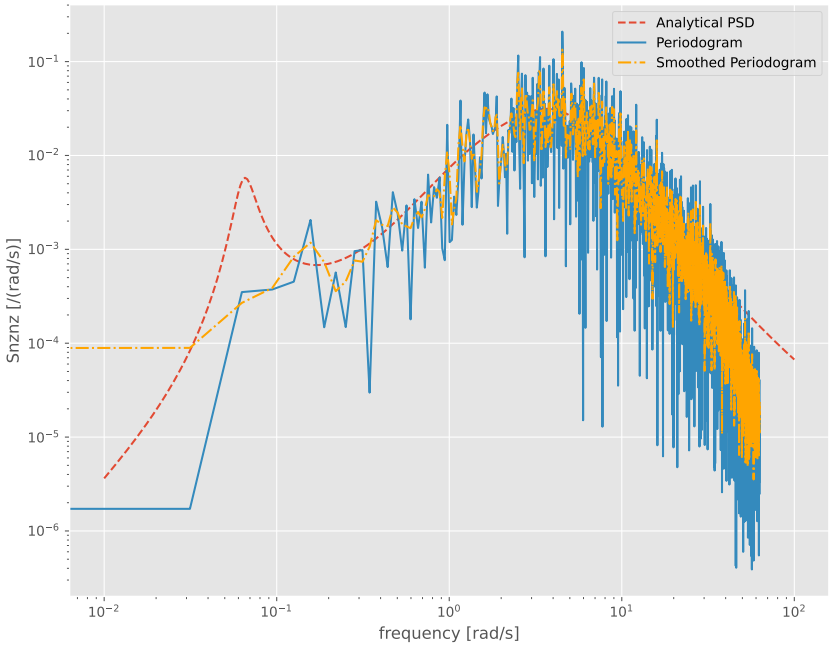

Figure 4.3: PSD of load factor for full system

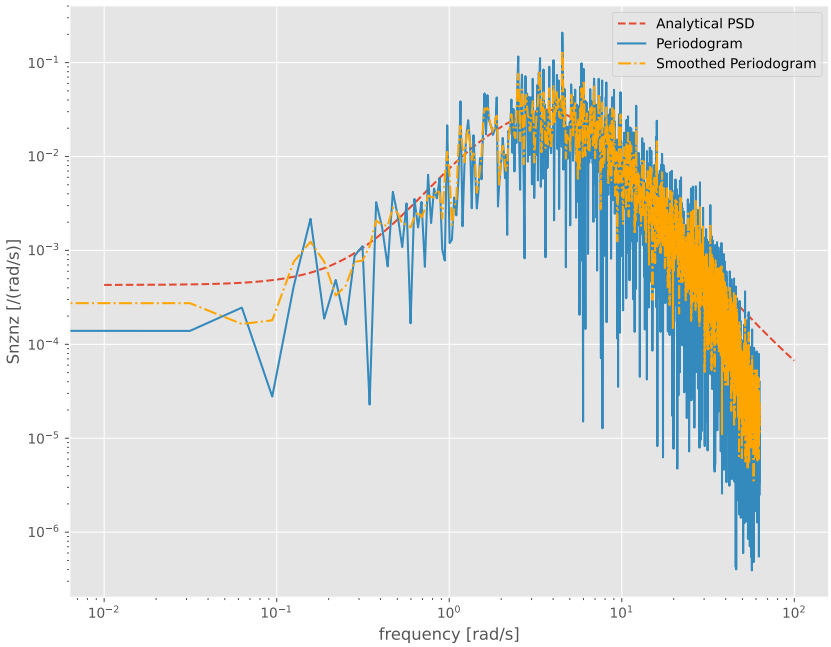

Figure 4.4: PSD of load factor for reduced system

The PSDs obtained through the analytical approach are found to be straight lines with no variations and this method is deterministic. Conversely, the experimental method displays a lot of fluctuations and is not uniform. The PSD estimated using fast Fourier transform (FFT) is based on a finite set of data points, and if the data length is insufficient, the PSD estimates may fluctuate. This is due to the fact that FFT assumes that the signal is periodic, and if the data length is insufficient, it may fail to accurately represent the periodicity of the signal, resulting in PSD fluctuations. Another reason for PSDs fluctuations is spectral leakage. It happens when the signal cannot fit integer times into the sampling period. PSD with smoothing filer only averages the signal out by taking the neighbouring numbers into account, however it does not prevent spectral leakage in any way. Lastly, the analytical PSD does not take input signal, that why it has straight lines, where as experimental PSD method takes in the input signal, which is also random and that contributes to the fluctuations.

Looking at the full system, the starting position of PSD for, $q\bar{c}/V$ (S_{qq}) and n_z (S_{nznz}) are quite off between the analytical method and experimental one, but from around 10^{-1} rad/s the PSDs start matching. One of possible reasons for this is that analytical method is not affected by input which is sampled randomly from standard normal distribution, while experimental method relies on it. By increasing the frequency, the signal-to-noise ration in the experimental method may improve, resulting to better agreement between the analytical and experimental PSDs. PSD for $\hat{u}$ (S_{uu}), $q\bar{c}/V$ (S_{qq}) and n_z (S_{nznz}) at higher frequencies (from around 10^{1}) can be seen that the slope becomes different for analytical method and experimental method. The slope depends on the order of the system, but in this case the system does not change. Time delays in the system can cause phase shifts in the frequency domain, which might not be captured by the analytical model, leading to discrepancies in the PSD slopes. For the reduced system, the starting position of PSDs seem to agree between the analytical method and the experimental one. The slope discrepancies also occurs for the $q\bar{c}/V$ state (S_{qq}) and n_z load factor (S_{nznz}).

PSD of α (S_{aa}) between full system and reduced are similar, but when looking at $q\bar{c}/V$ (S_{qq}) there are some differences, especially for analytical methods. The starting position is a three-magnitude difference and there is a bump at around $7 \cdot 10^{-2}$ rad/s for the full system, while no bump can be examined at that frequency for the reduced system. For the n_z load factor (S_{nznz}) is similar situation: two-magnitude difference at the starting point and also no bump for the reduced system at again around $7 \cdot 10^{-2}$ rad/s. The reduced system is a simplified version of the full system, where certain dynamics and components have been removed (Equation 2.3). This simplification may lead to differences in the PSD of $q\bar{c}/V$ (S_{qq}) between the full and reduced systems, as some frequency components may be missing or represented differently in the reduced system.

5
Variances

This chapter presents results of estimated variances of aircraft states and load factor for both aircraft models. Three methods were applied to estimate the variance: analytical power spectra method, impulse response method and Matlab routine var.m method. The Matlab method was replaced with equivalent numpy.var method since the analyses was done with Python. The variance with the analytical power spectra method is calculated by integrating PSD and then dividing by π. Formula is give in Equation 5.1. PSD values are taken from chapter 4

$$\sigma_x^2 = \frac{1}{\pi}\int_0^\infty S_{xx}(\omega)d\omega \tag{5.1}$$

The next method is impulse response method. This is done by simulating the output of a linear system with zero input and selecting initial condition to second or third column of B matrix ($x(0) = B_i$ second column corresponds to vertical turbulence input and third column to longitudinal turbulence input). The output is squared and integrated. Adding variances due to vertical turbulence input and longitudinal turbulence input, the final variance is computed. Formula for this method can be seen in Equation 5.2, where h_{ji} is the output for j state and i input.

$$\sigma_{x_j}^2(t) = \sum_{i=1}^{m}\int_0^t h_{ji}^2(v)dv \tag{5.2}$$

The final method is numpy built in variance function. Equation 5.3 is used to calculate the variance.

$$\begin{aligned}\sigma_x^2 &= \frac{1}{N-1}\sum_{i=1}^{N}|X_i - \mu_x|^2 \\ \mu_x &= \frac{1}{N}\sum_{i=1}^{N}X_i\end{aligned} \tag{5.3}$$

The calculated variances for both the complete and reduced system are shown in Table 5.1 and Table 5.2. Differences can be observed among the outcomes of various methods. The analytical power spectra method computes the variance from the analytical PSD, which is constructed using the Bode plots of the state variables in relation to vertical and longitudinal turbulence inputs. The analytical curve exhibits minimal fluctuations, allowing for a uniform calculation of the area beneath it. The inputs for the numpy var method are derived from the system output after applying the lsim command to the state space matrices. Same goes for the impulse response method. These inputs are accompanied by significant noise, leading to a rough approximation of the area and resulting in differences between the three methods. When comparing the results between the full system and reduced one, the differences are relatively small, except for α state with impulse response method, where the difference is one order of magnitude.

Table 5.1: Variances of the state variables for the full system

Method	$\hat{u}[-]$	$\alpha\ [rad^2]$	$\theta\ [rad^2]$	$q\bar{c}/V\ [rad^2]$	n_z [-]
Analytical power spectra	2.312×10^{-5}	8.724×10^{-5}	6.256×10^{-5}	2.089×10^{-8}	7.421×10^{-2}
Impulse response method	2.273×10^{-5}	8.618×10^{-5}	6.079×10^{-5}	2.258×10^{-8}	1.711×10^{-1}
NumPy routine numpy.var	5.233×10^{-6}	8.804×10^{-5}	4.130×10^{-5}	1.916×10^{-8}	8.464×10^{-4}

Table 5.2: Variances of the state variables for the reduced system

Method	$\alpha\ [rad^2]$	$q\bar{c}/V\ [rad^2]$	n_z [-]
Analytical power spectra	8.720×10^{-5}	2.085×10^{-8}	7.422×10^{-2}
Impulse response method	1.723×10^{-4}	4.499×10^{-8}	1.709×10^{-1}
NumPy routine numpy.var	8.802×10^{-5}	1.912×10^{-8}	8.464×10^{-4}

6
Conclusion

In the report it was examined the impact of symmetrical atmospheric turbulence on a rigid aircraft, focusing on the vertical and longitudinal turbulence components. In chapter 2, the full and reduced aircraft models were analysed and eigenvalues were computed to determine their stability. Both models found to be stable as no eigenvalues had a positive real component

In chapter 3, both the full model and the reduced model were simulated over a period of 60 seconds to obtain the time behaviour of the system state variables. chapter 4 presented the spectral analysis of the aircraft states and load factor, using analytical, experimental, and experimental with smoothing filter methods. The outcomes of each method varied, and the reasons for these variations were explained alongside the results.

Finally, in chapter 5 the variances of aircraft state variables and the load factor component were determined using three different methods: analytical power spectra, impulse response and numpy.var methods. The simulation results for variances differ to some extent due to the randomisation considered when constructing the turbulence input components.

In conclusion, this assignment has successfully achieved its objectives of enhancing the comprehension of aircraft dynamics under turbulent conditions and showcasing the adaptability of time and frequency domain analysis methods in the study of diverse stochastic processes. Ultimately, the knowledge and experience gained through this assignment can be applied to other real-world systems and engineering applications, emphasising the importance and relevance of these analysis techniques in a broader context.

Bibliography

[1] J. A. Mulder, J. C. Van der Vaart, W. Van Staveren, Q. Chu, and M. Mulder, *Aircraft responses to atmospheric turbulence*, Lecture notes AE4304.

[2] W. Van Staveren, J. Van der Vaart, E. De Weerdt, and J. Mulder, *Flight dynamics*, Lecture notes AE3302.